Supporting Information for:

Immobilization of Molecular Catalysts on Solid Supports via Atomic Layer Deposition for Chemical Synthesis in Sustainable Solvents

Pooja J. Ayare[#], Shawn A. Gregory[†], Ryan J. Key[#], Andrew E. Short[†], Jake G. Tillou[#], James D. Sitter[#], Typher Yom[†], Dustin W. Goodlett[#], Dong-Chan Lee[†], Faisal M. Alamgir[†], Mark D. Losego[†]*, and Aaron K. Vannucci[#]*

[#]Department of Chemistry and Biochemistry, University of South Carolina, Columbia, SC 29208, USA

[†]Department of Materials Science & Engineering, Georgia Institute of Technology, Atlanta, GA 30332, USA

Corresponding Author

* E-mail: vannucci@mailbox.sc.edu losego@gatech.edu

Table of Contents

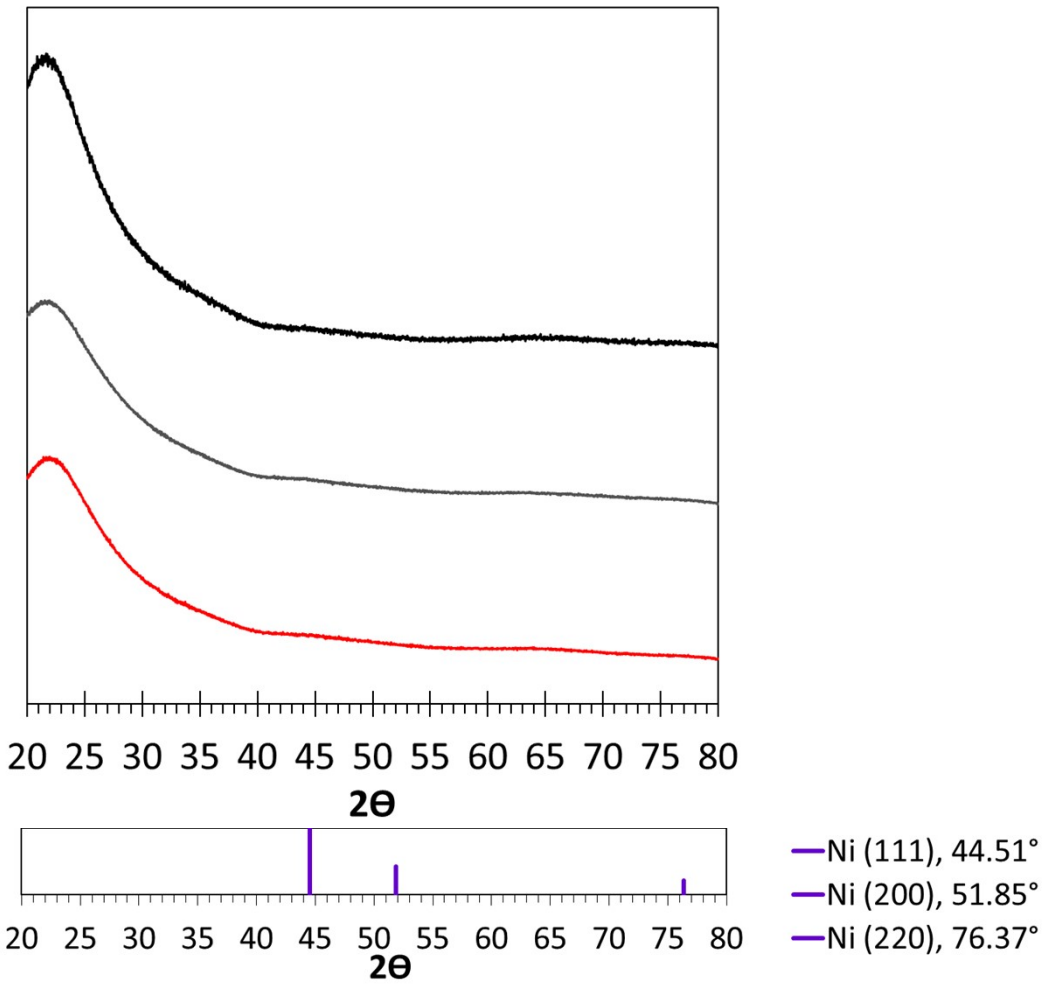

Figure S1. Top: XRD data for **1**|SiO_2 (black), **1**|SiO_2|TiO_2 pre-reaction (gray), and **1**|SiO_2|TiO_2 post-reaction (red). All three patterns show the amorphous silica support without any evidence for nickel nanoparticles. Bottom: Predicted signals for nickel nanoparticles.

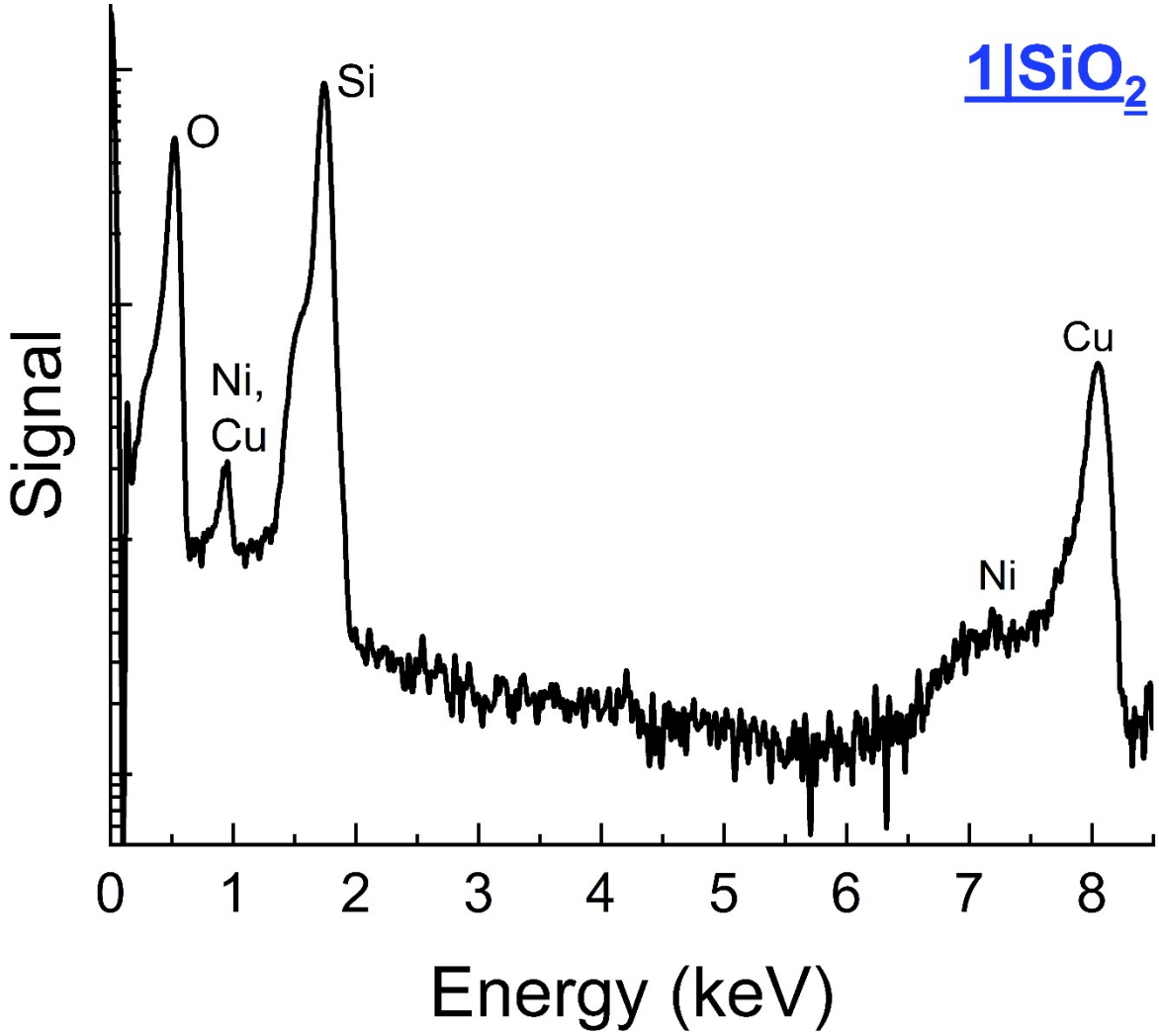

Figure S2. EDS elemental analysis of **1|SiO_2** before atomic layer deposition. Individual elements are labeled for clarity. Note that the y-axis is a logarithmic scale because Si and O are orders of magnitude more abundant than Ni. Additionally, the Cu signal is from the copper grid used to hold samples in the STEM instrument. Lastly, carbon and nitrogen are likely present at *ca.* 0.27 and 0.39 keV, but these peaks are difficult to resolve and assign.

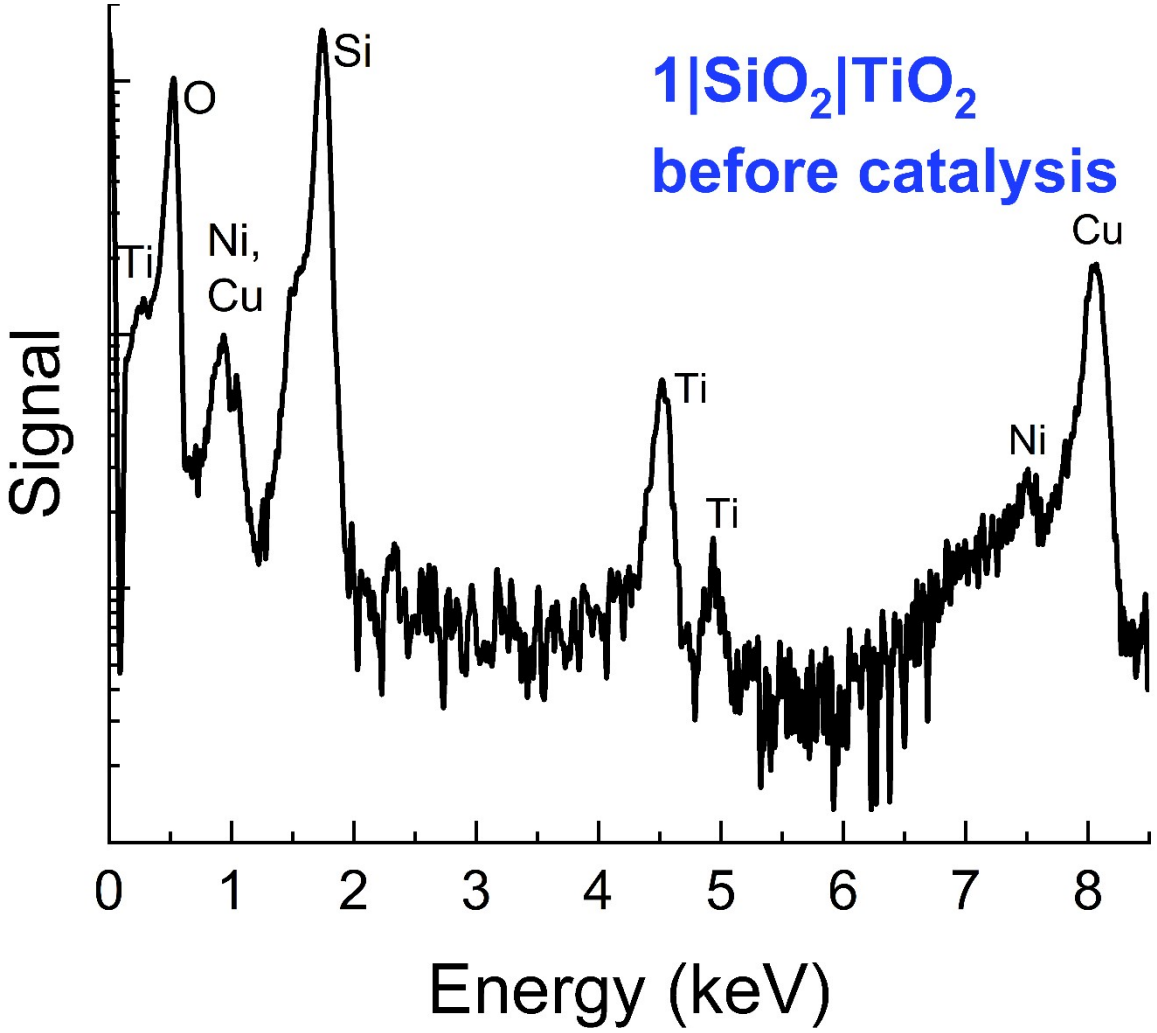

Figure S3. EDS elemental analysis of **1|SiO_2|TiO_2** after $TiCl_4$ + H_2O atomic layer deposition but before catalytic reactions. Figure S3 more clearly shows Ni signal in comparison to Figure S2, and Figure S3 also confirms the presence of titania coating. This is consistent with ICPMS, found in Table 3.

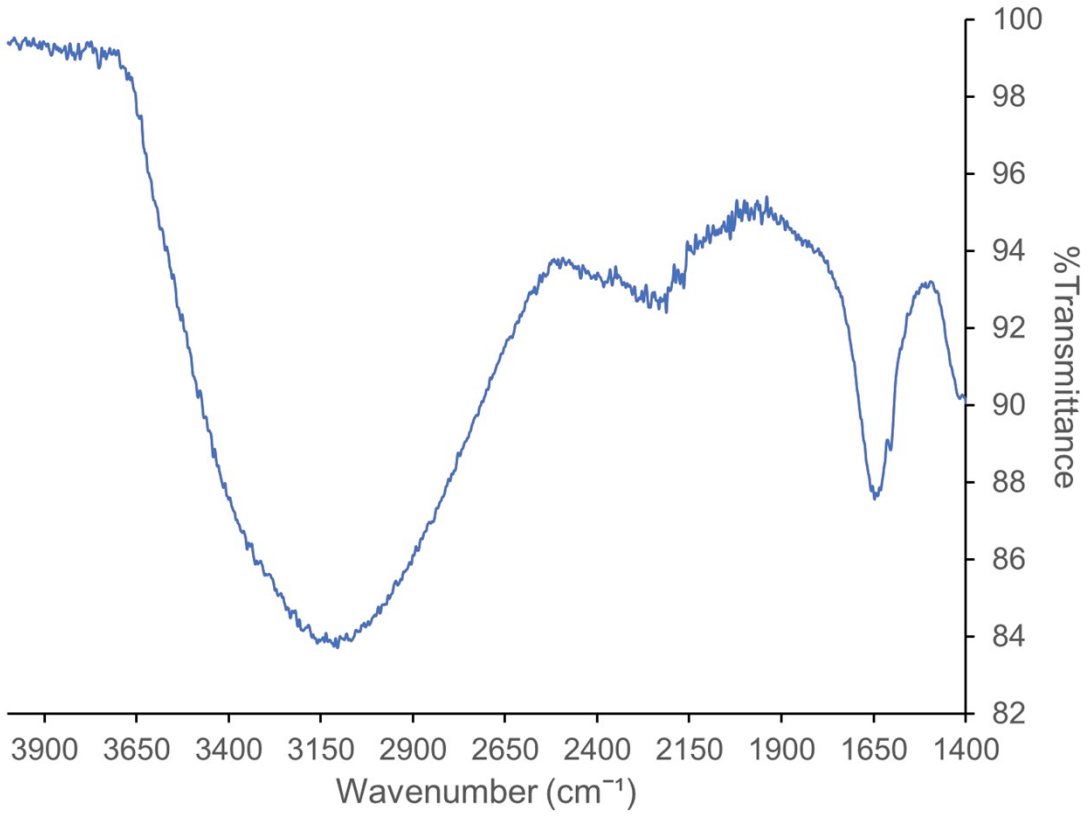

Figure S4. FTIR-ATR spectrum of **1|SiO_2|TiO_2** post-reaction showing the C-O stretching frequency below 1650 cm^{-1} attributed to catalyst ligand binding to the oxide support.

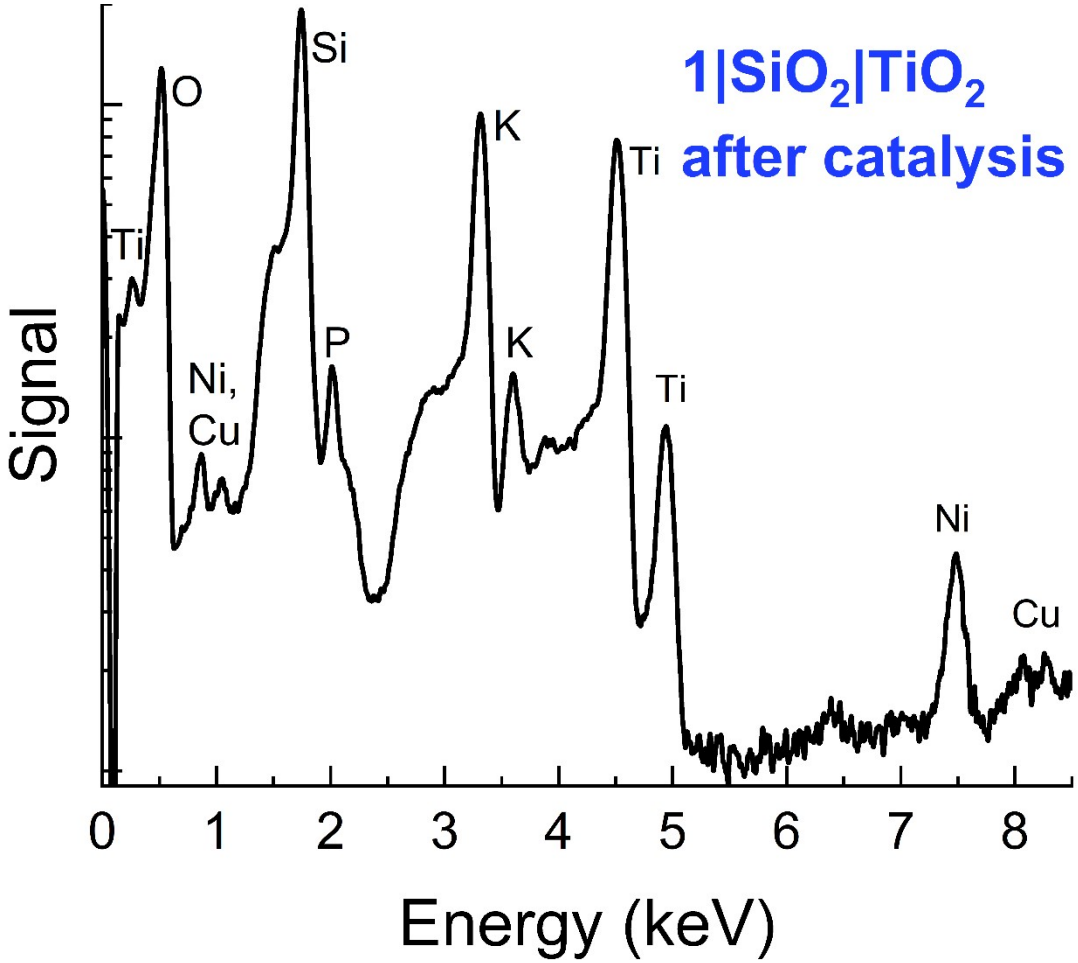

Figure S5. EDS elemental analysis of **1|SiO_2|TiO_2** after $TiCl_4$ + H_2O atomic layer deposition and after catalytic reactions. **Figure S5** shows that Ni is still present on the hybrid catalyst powder, consistent with ICPMS in Table 3. Additionally, K and P signals are present, and we attribute their presence to residual K_3PO_4, from the buffer used in the catalytic reactions (see Table 2 and Table 3).

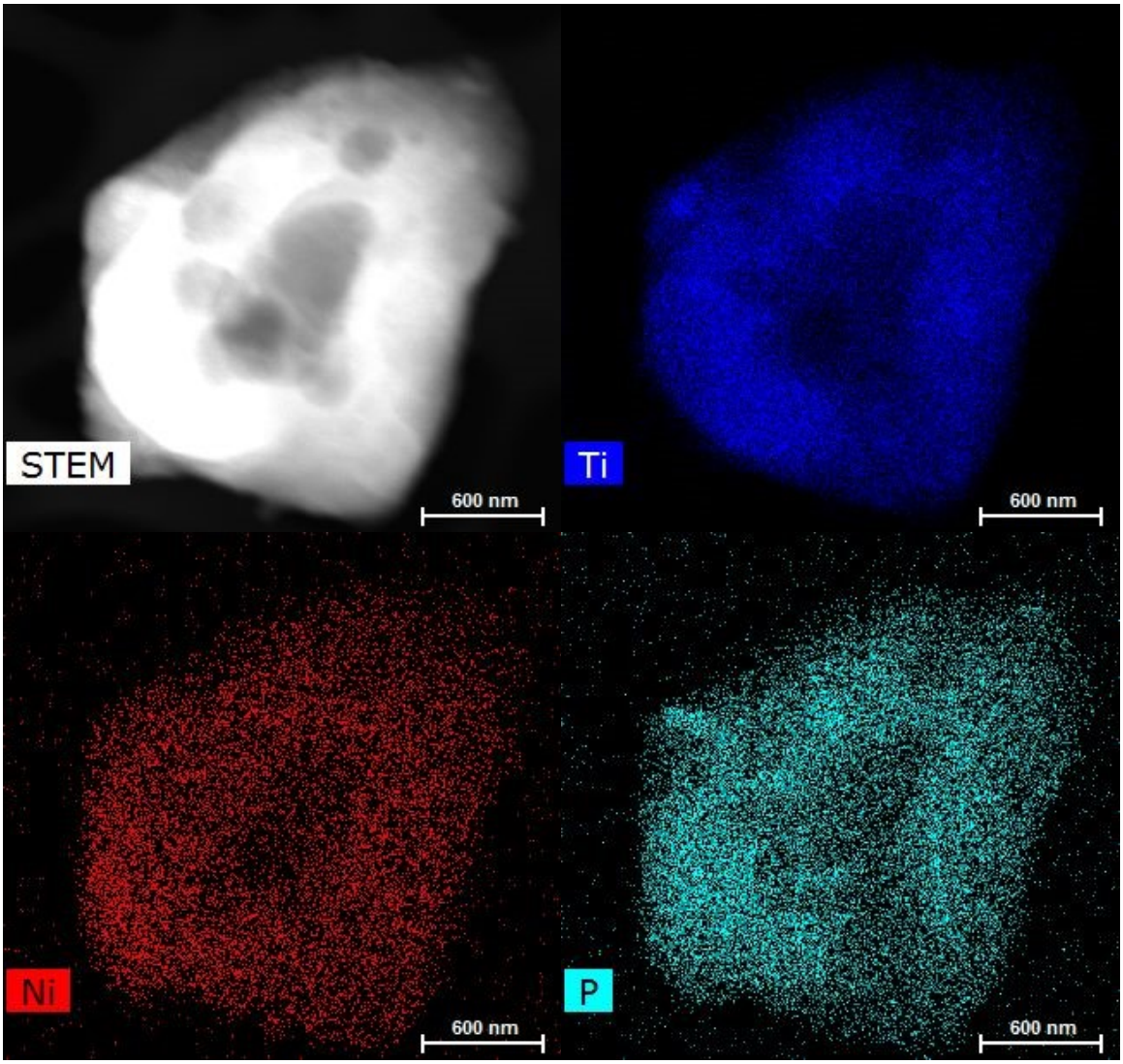

Figure S6. STEM image of **1**|SiO_2|TiO_2 and elemental maps of Ti, Ni, and P detected post-reaction.

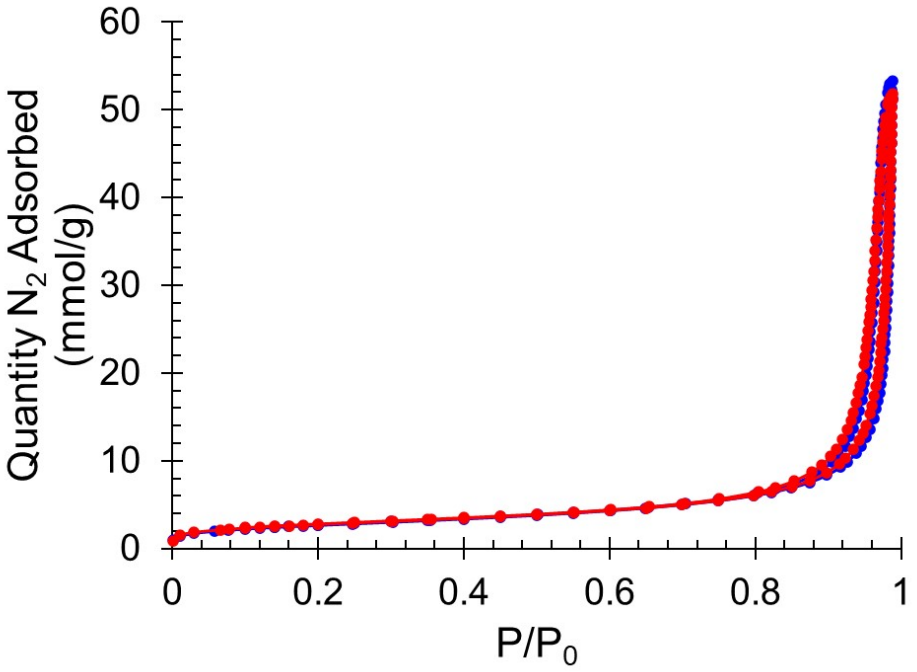

Figure S7. N_2 adsorption/desorption isotherms for **1|SiO$_2$** (pre-ALD, blue), and **1|SiO$_2$|TiO$_2$** (10 cycles ALD, red).

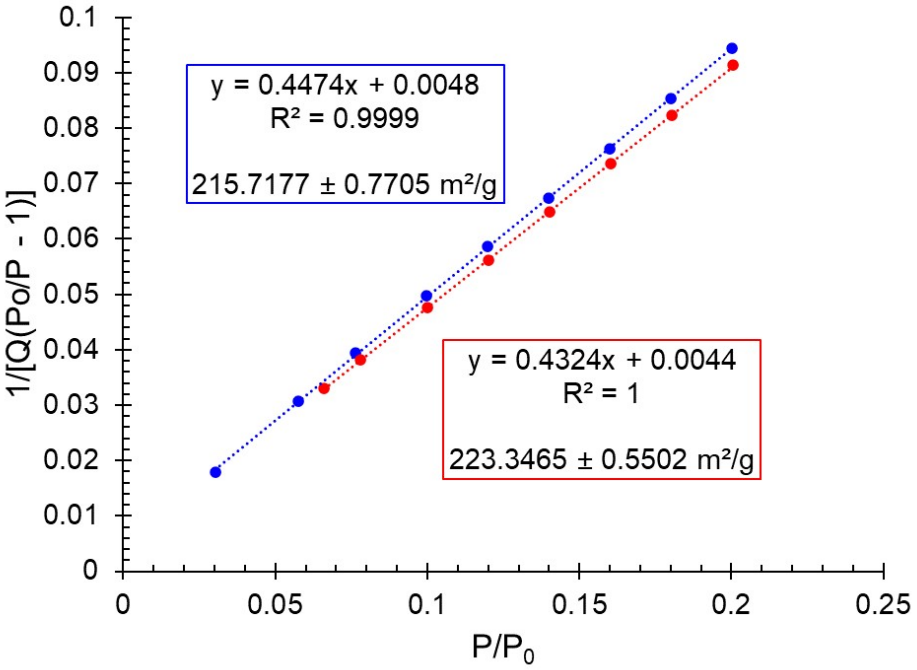

Figure S8. BET transformation of N_2 isotherm data for **1|SiO$_2$** (pre-ALD, blue), and **1|SiO$_2$|TiO$_2$** (10 cycles ALD, red).

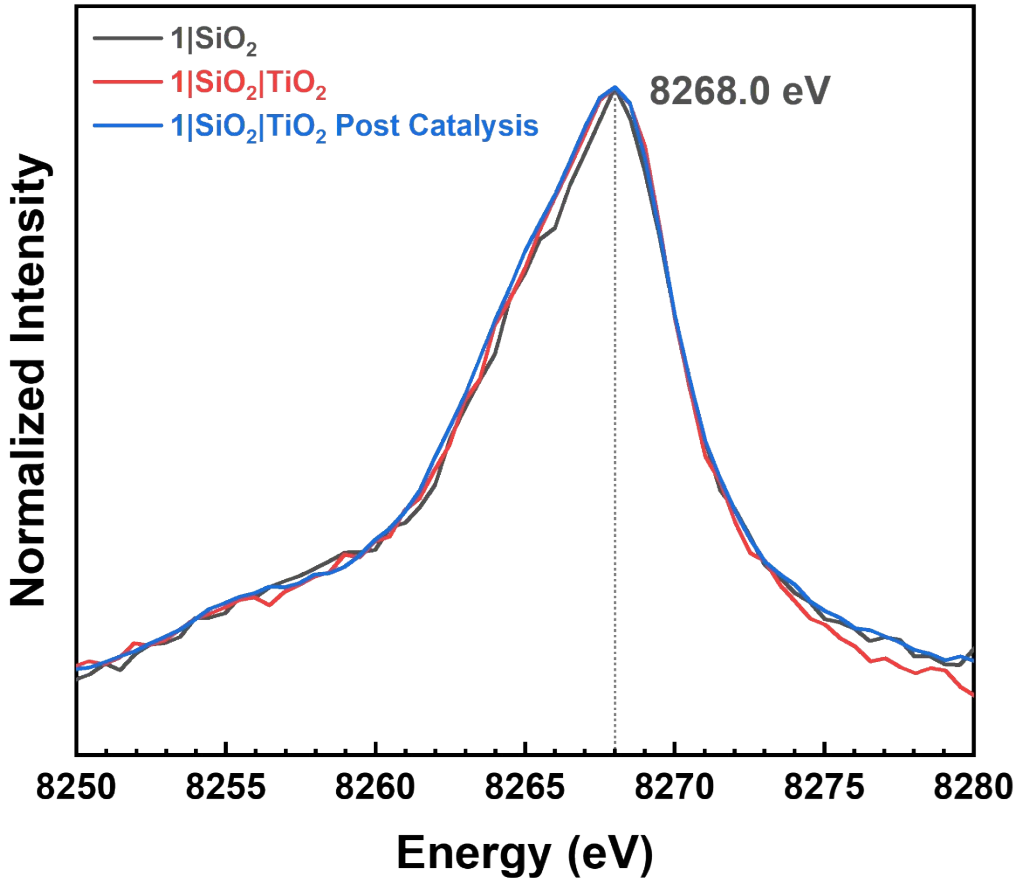

Figure S9. Normalized Ni Kβ XES spectra overlays of **1|SiO$_2$** (no ALD coating), **1|SiO$_2$|TiO$_2$** (with ALD overcoating, pre-reaction, and **1|SiO$_2$|TiO$_2$** (with ALD coating, post 24 hour cross-coupling reaction).

Over the course of 5 consecutive 24-hour reactions the hybrid ALD catalyst exhibits consistent catalytic activity and product formation. The summation of the products obtained from each reaction equates to roughly 500 catalytic turnovers without a considerably observed decrease in product formation over time (percent yields for each reaction range between 84% and 90%). Conversely, the **1**|**SiO$_2$** catalyst produces a minimal number of turnovers (~25) in the first reaction and then deactivates, resulting in no additional turnovers.

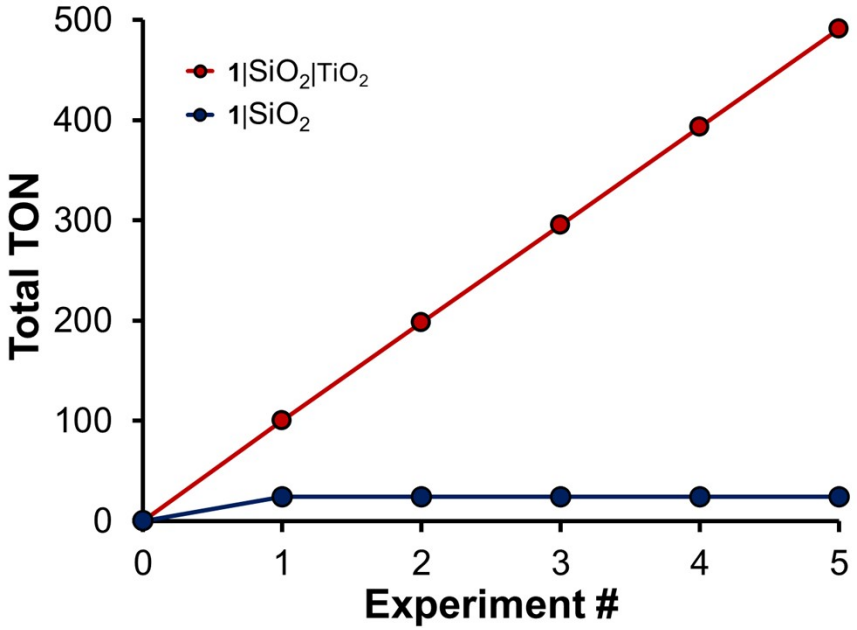

Figure S10. Total summed turnover number (TON) vs. consecutive cross-coupling reactions of **1**|**SiO$_2$**|**TiO$_2$** (red) and **1**|**SiO$_2$** (blue). Experimental conditions are described in Table 1.

List of ^{1}H & ^{13}C NMR peaks of products

Multiplicity was indicated as follows: s (singlet), d (doublet), t (triplet), q (quartet), m (multiplet).

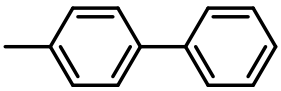

^{1}H NMR (DMSO, 300 MHz) δ 2.62 (s, 3H), 7.46 (d, *J* = 9.0 Hz, 2H), 7.55-7.57 (m, 1H), 7.63 (t, *J* = 7.3 Hz, 2H), 7.71-7.74 (d, *J* = 9.0 Hz, 2H), 7.80-7.82 (m, 2H). ^{13}C NMR ($CDCl_3$, 300 MHz) δ (ppm): 21.13, 127.00, 128.74, 129.51, 131.23, 137.05, 138.39, 141.19.

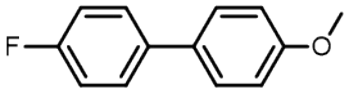

^{1}H NMR (CD_2Cl_2, 300 MHz) δ 3.84 (s, 3H), 6.96-6.99 (m, 2H), 7.09-7.15 (m, 2H), 7.48-7.55 (m, 4H). ^{13}C NMR (CD_2Cl_2, 300 MHz) δ (ppm): 55.28, 114.18, 115.27, 115.55, 127.91, 128.20, 132.55, 136.95, 159.25, 163.69.

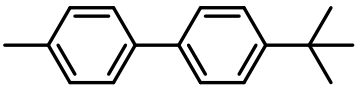

^{1}H NMR ($CDCl_3$, 300 MHz) δ 1.37 (s, 9H), 2.40 (s, 3H), 7.24-7.26 (d, *J* = 7.9 Hz, 2H), 7.45-7.55 (m, 6H). ^{13}C NMR ($CDCl_3$, 300 MHz) δ (ppm): 21.11, 31.39, 34.51, 125.67, 126.60, 126.87, 129.43, 131.21, 136.71, 137.24, 138.26.

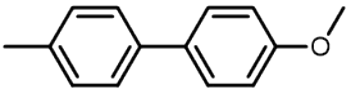

^{1}H NMR (CD_2Cl_2, 300 MHz) δ 2.36 (s, 3H), 3.82 (s, 3H), 6.94-6.96 (d, *J* = 8.8 Hz, 2H), 7.20-7.23 (d, *J* = 8.0 Hz, 2H), 7.43-7.46 (d, *J* = 8.13, 2H), 7.49-7.52 (d, *J* = 8.8 Hz, 2H). ^{13}C NMR (CD_2Cl_2, 300 MHz) δ (ppm): 20.72, 55.26, 114.10, 126.35, 127.75, 129.39, 133.47, 136.46, 137.74, 159.05.

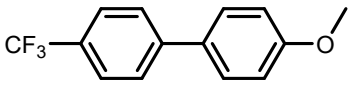

^{1}H NMR (DMSO, 300 MHz) δ 3.85 (s, 3H), 6.99-7.02 (d, *J* = 8.6 Hz, 2H), 7.56-7.59 (d, *J* = 8.6 Hz, 2H), 7.65-7.71 (m, 4H). ^{13}C NMR ($CDCl_3$, 300 MHz) δ (ppm): 55.33, 114.09, 114.36, 125.62, 126.82, 127.53, 128.28, 160.30.

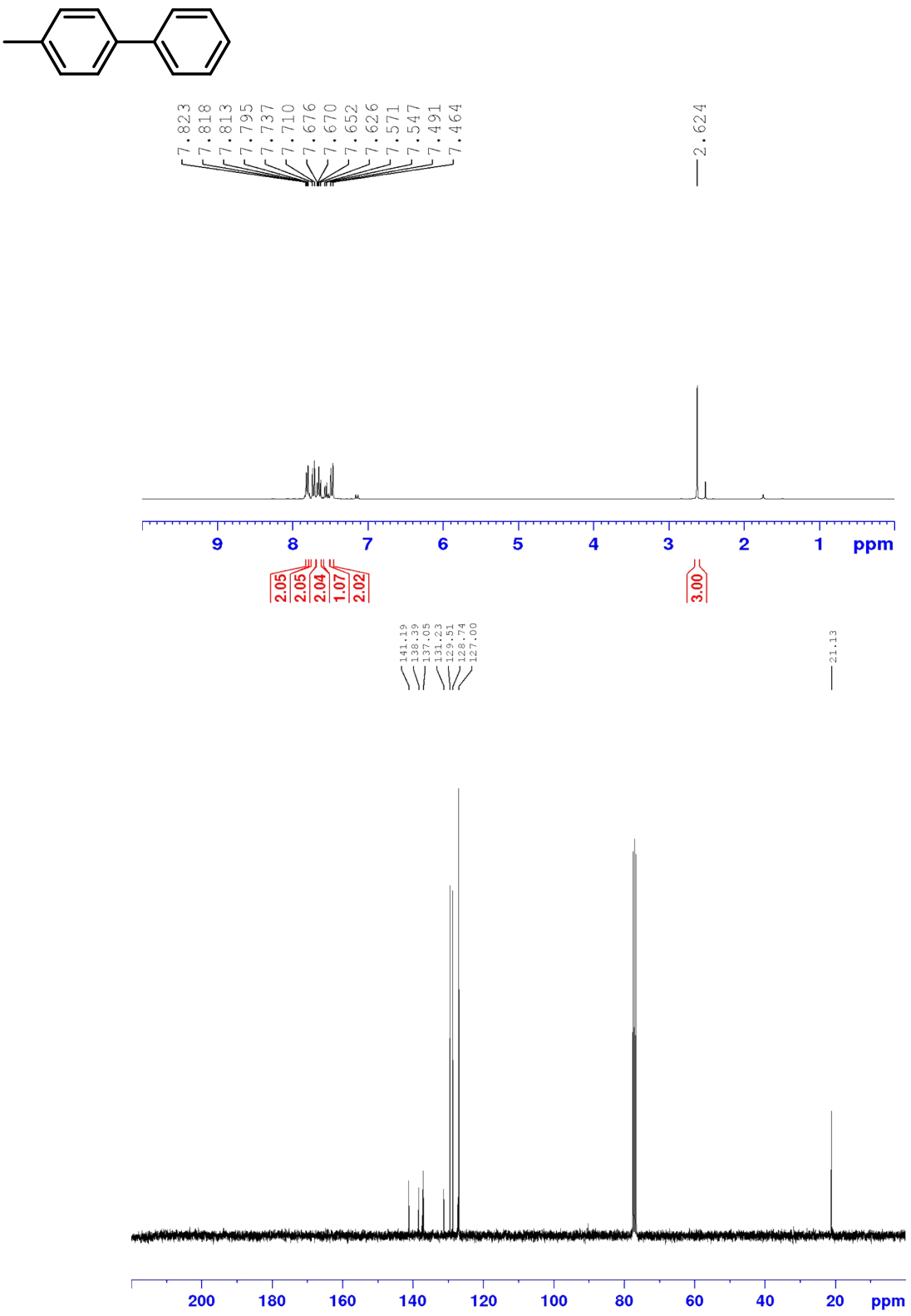

Figure S11: ^{1}H and ^{13}C NMR of 4-Methyl-1,1'-biphenyl which matches the previously reported spectra.[1]

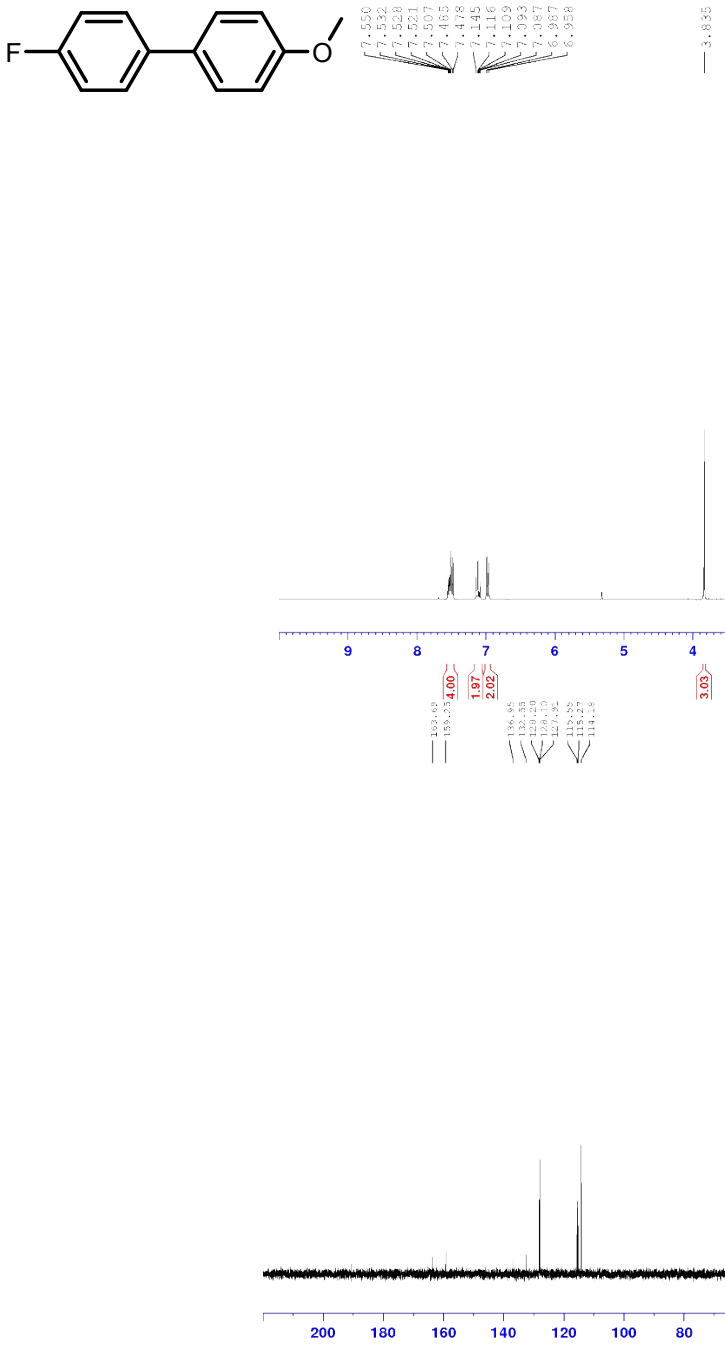

Figure S12: ^{1}H and ^{13}C NMR of 4-Fluoro-4'-methoxy-1,1'-biphenyl which matches the previously reported spectra.[2]

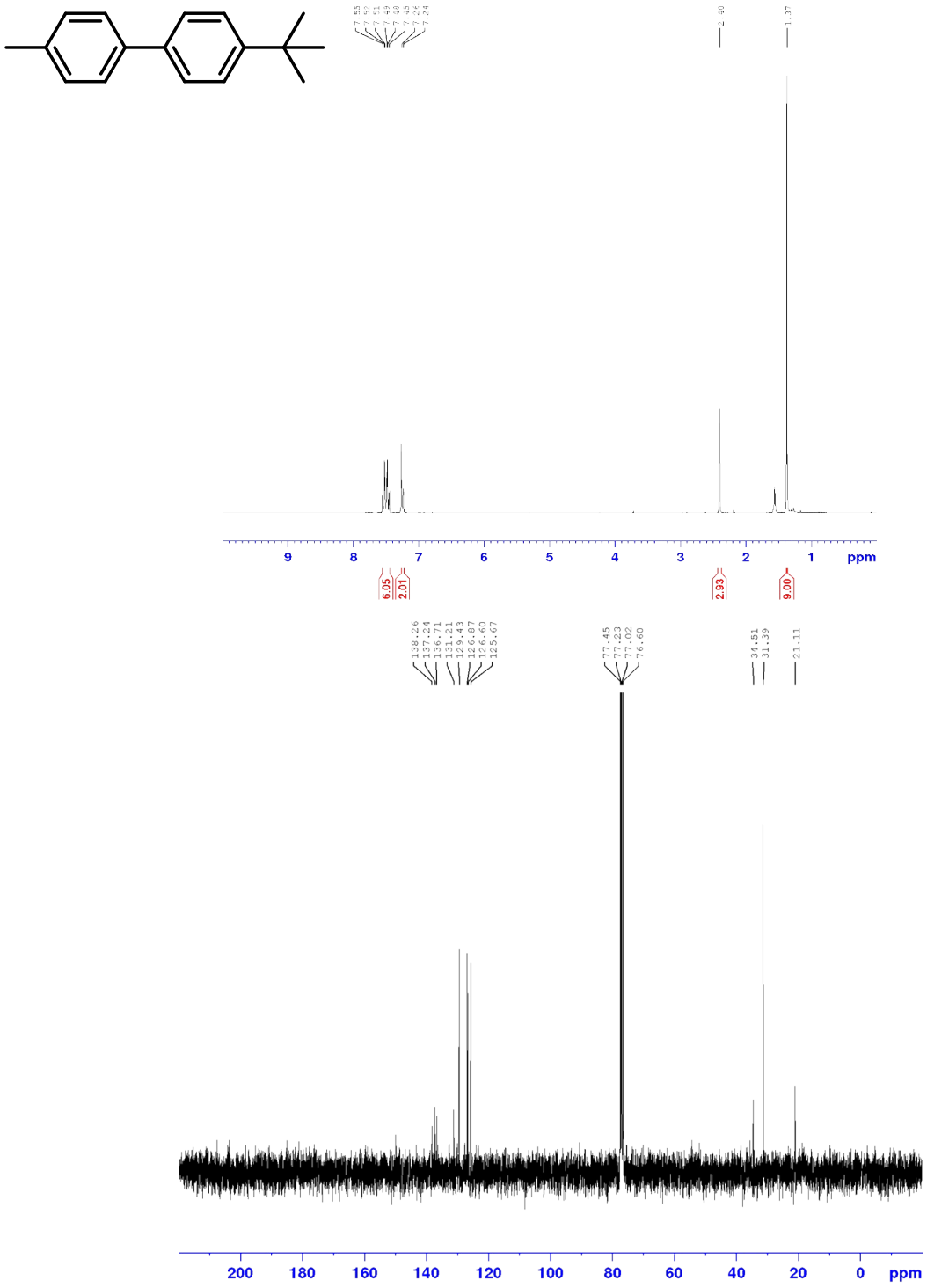

Figure S13: ^{1}H and ^{13}C NMR of 4-(*tert*-butyl)-4'-methyl-1,1'-biphenyl which matches the previously reported spectra.[1]

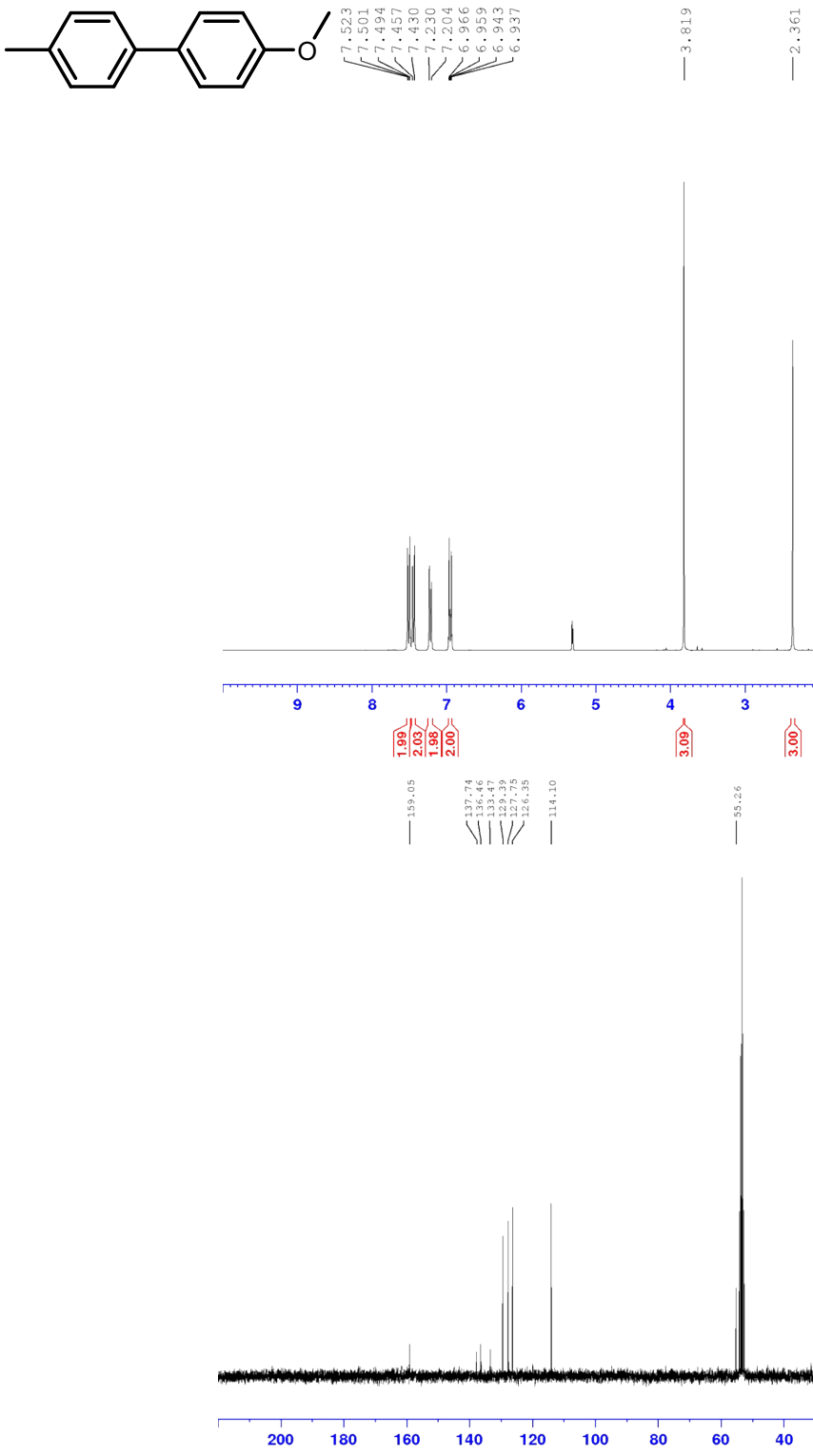

Figure S14: ^{1}H and ^{13}C NMR of 4-methoxy-4'-methyl-1,1'-biphenyl which matches the previously reported spectra.[1]

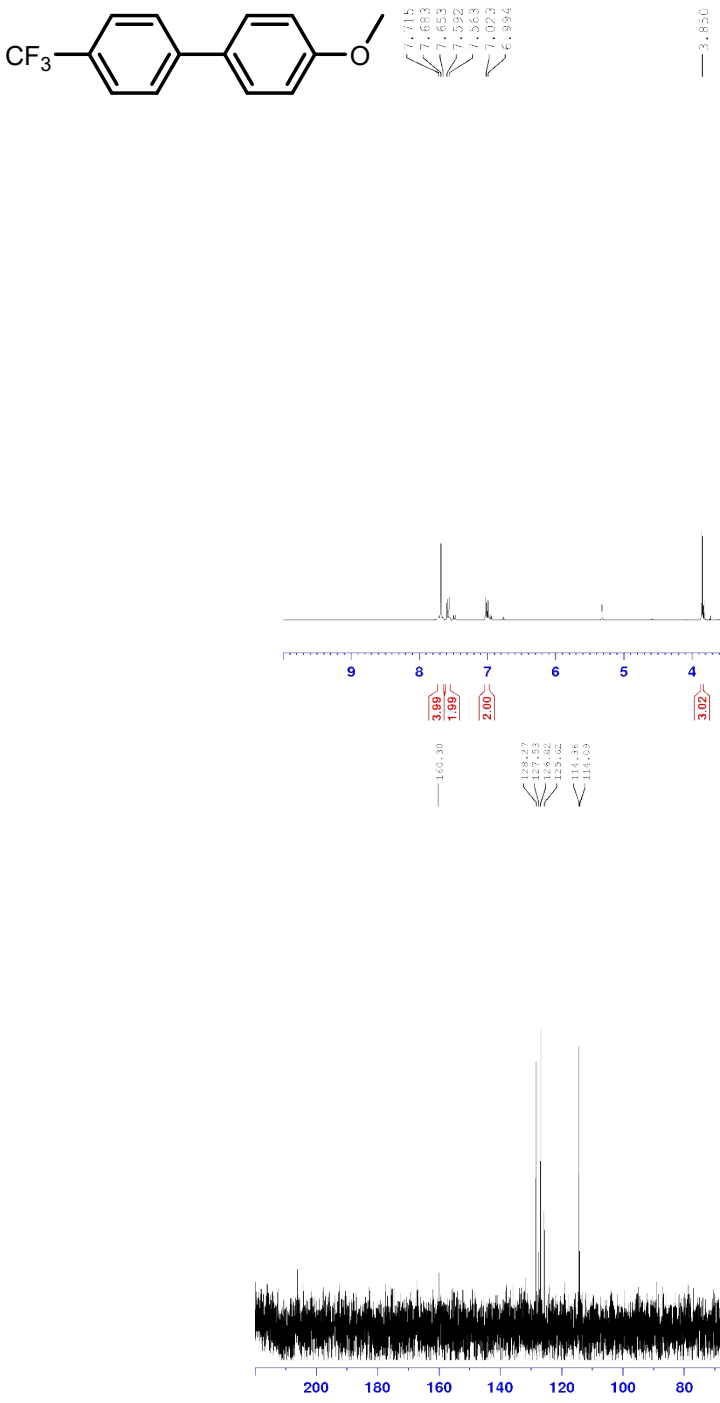

Figure S15: ^{1}H and ^{13}C NMR of 4-methyl-4'-(trifluoromethyl)-1,1'-biphenyl which matches the previously reported spectra.[3]

References:

1. P. Y. Choy, O. Y. Yuen, M. P. Leung, W. K. Chow, and F. Y. Kwong. *Eur. J. Org. Chem.* 2020, 2846-2853.
2. I. D. Inaloo, S. Majnooni, H. Eslahi, and M. Esmaeilpour. *ACS Omega,* 2020, **5**, 7406-7417.
3. C. P. Delaney, V. M. Kassel, and S. E. Denmark. *ACS Catal.*, 2020, **10***,* 73-80.